



# On the Single-event-based Identification of Primordial Black Hole Mergers at Cosmological Distances

Ken K. Y. Ng<sup>1,2</sup> , Shiqi Chen<sup>1,2</sup>, Boris Goncharov<sup>3,4</sup> , Ulyana Dupletsa<sup>3,4</sup>, Ssohrab Borhanian<sup>5,6</sup> , Marica Branchesi<sup>3,4</sup>, Jan Harms<sup>3,4</sup> , Michele Maggiore<sup>7</sup> , B. S. Sathyaprakash<sup>5,8,9</sup> , and Salvatore Vitale<sup>1,2</sup>

<sup>1</sup>LIGO, Massachusetts Institute of Technology, Cambridge, MA 02139, USA; [kenkyng@mit.edu](mailto:kenkyng@mit.edu)

<sup>2</sup>Kavli Institute for Astrophysics and Space Research, Department of Physics, Massachusetts Institute of Technology, Cambridge, MA 02139, USA

<sup>3</sup>Gran Sasso Science Institute (GSSI), I-67100 L'Aquila, Italy

<sup>4</sup>INFN, Laboratori Nazionali del Gran Sasso, I-67100 Assergi, Italy

<sup>5</sup>Institute for Gravitation and the Cosmos, Department of Physics, Pennsylvania State University, University Park, PA 16802, USA

<sup>6</sup>Theoretisch-Physikalisches Institut, Friedrich-Schiller-Universität Jena, D-07743, Jena, Germany

<sup>7</sup>Département de Physique Théorique and Center for Astroparticle Physics, Université de Genève, 24 quai Ansermet, CH-1211 Genève 4, Switzerland

<sup>8</sup>Department of Astronomy & Astrophysics, Pennsylvania State University, University Park, PA 16802, USA

<sup>9</sup>School of Physics and Astronomy, Cardiff University, Cardiff, CF24 3AA, UK

Received 2022 February 22; revised 2022 April 19; accepted 2022 April 29; published 2022 May 23

## Abstract

The existence of primordial black holes (PBHs), which may form from the collapse of matter overdensities shortly after the Big Bang, is still under debate. Among the potential signatures of PBHs are gravitational waves (GWs) emitted from binary black hole (BBH) mergers at redshifts  $z \gtrsim 30$ , where the formation of astrophysical black holes is unlikely. Future ground-based GW detectors, the Cosmic Explorer and Einstein Telescope, will be able to observe equal-mass BBH mergers with total mass of  $\mathcal{O}(10\text{--}100) M_{\odot}$  at such distances. In this work, we investigate whether the redshift measurement of a single BBH source can be precise enough to establish its primordial origin. We simulate BBHs of different masses, mass ratios and orbital orientations. We show that for BBHs with total masses between  $20 M_{\odot}$  and  $40 M_{\odot}$  merging at  $z \geq 40$ , one can infer  $z > 30$  at up to 97% credibility, with a network of one Einstein Telescope, one 40 km Cosmic Explorer in the US, and one 20 km Cosmic Explorer in Australia. This number reduces to 94% with a smaller network made of one Einstein Telescope and one 40 km Cosmic Explorer in the US. We also analyze how the measurement depends on the Bayesian priors used in the analysis and verify that priors that strongly favor the wrong model yield smaller Bayesian evidences.

*Unified Astronomy Thesaurus concepts:* Gravitational waves (678); Primordial black holes (1292); Astrophysical black holes (98); Stellar mass black holes (1611)

## 1. Introduction

The formation of primordial black holes (PBHs) was suggested more than five decades ago (Zel'dovich & Novikov 1966; Hawking 1971; Carr & Hawking 1974), but these hypothetical compact objects still elude discovery. Unlike astrophysical black holes (ABHs)—which are stellar remnants—PBHs are formed by the direct collapse of matter overdensities in the early universe (Ivanov et al. 1994; Garcia-Bellido et al. 1996; Ivanov 1998). See also Polnarev & Khlopov (1985), Khlopov (2010), Sasaki et al. (2016), and Green & Kavanagh (2021) for reviews. While there are significant uncertainties in their mass spectrum, Carr & Hawking (1974), Carr et al. (2017), and Ali-Haïmoud et al. (2017) suggest that PBHs may occur in the range  $\mathcal{O}(1\text{--}100)M_{\odot}$ . Stellar-mass PBHs could form binaries (Nakamura et al. 1997; Ioka et al. 1998) that merge and emit gravitational waves (GWs) detectable by current GW detectors, including LIGO, Virgo, and KAGRA (LVK) (Aso et al. 2013; Aasi et al. 2015; Acernese et al. 2015) and leave a unique imprint on the mass spectrum and redshift evolution in the observable population of binary black hole (BBH) mergers (Ali-Haïmoud et al. 2017; Clesse & Garcia-Bellido 2017; Raidal et al. 2017, 2019; Chen & Huang 2018; Belotsky et al. 2019; De Luca et al. 2020a, 2020b). Efforts have been made to test if a fraction of the BBHs in the

LVK's second catalog (Abbott et al. 2021) could be of primordial origin by analyzing the population properties of BBH mergers detected thus far (De Luca et al. 2020c; Franciolini et al. 2022; Hütsi et al. 2021; Mukherjee & Silk 2021; Wong et al. 2021). However, even at design sensitivity, the horizon of current GW detectors will be limited to redshifts of  $z \lesssim 3$  at most (Hall & Evans 2019). Interpreting these “local” observations, with the aim of establishing the presence of a PBH subpopulation, requires precise knowledge of the ABH population, which is dominant at low redshifts and acts as an “astrophysical foreground” (Franciolini et al. 2022). This is challenging, as there exist significant uncertainties on the properties of BBHs formed in different astrophysical environments, such as galactic fields (Dominik et al. 2012, 2013, 2015; de Mink & Belczynski 2015; Belczynski et al. 2016; O’Shaughnessy et al. 2017; Stevenson et al. 2017; Broekgaarden et al. 2019; Mapelli et al. 2019; Bavera et al. 2020; Breivik et al. 2020), dense star clusters (Rodríguez et al. 2015, 2016; Rodríguez & Loeb 2018; Di Carlo et al. 2019; Antonini & Gieles 2020; Kremer et al. 2020; Portegies Zwart & McMillan 2000; Santoliquido et al. 2021), active galactic nuclei (Bartos et al. 2017; Yang et al. 2019, 2020; Yi & Cheng 2019; Gröbner et al. 2020; Samsing et al. 2020; Tagawa et al. 2020a, 2020b, 2021), or from the collapse of Population III stars (Kinugawa et al. 2014, 2016; Hartwig et al. 2016; Belczynski et al. 2017).

One can ascertain the primordial origin of black holes by detecting mergers at redshifts so high that ABHs could not have had the time to form and merge yet. A plausible lower



Original content from this work may be used under the terms of the [Creative Commons Attribution 4.0 licence](https://creativecommons.org/licenses/by/4.0/). Any further distribution of this work must maintain attribution to the author(s) and the title of the work, journal citation and DOI.

bound for this redshift would be  $z \sim 30$  (see discussion below). Therefore, measuring the redshift of a BBH merging at redshifts larger than 30 would be a clear hint of the existence of PBHs (De Luca et al. 2021a, 2021b).

Proposed next-generation, ground-based GW detectors such as the Cosmic Explorer (CE) (Abbott et al. 2017; Reitze et al. 2019; Evans et al. 2021a) and the Einstein Telescope (ET) (Punturo et al. 2010; Maggiore et al. 2020) can detect BBH mergers at  $z > 10$  and above (Hall & Evans 2019). However, being able to detect a source merging at redshift larger than 30 does not automatically imply being able to prove that the true redshift was above some threshold. The purpose of this Letter is to systematically study how well next-generation GW detectors can measure the redshift of distant BBHs.

## 2. Simulations

Given the significant uncertainty in the mass spectrum of PBHs, we consider a range of values that would lead to detectable GW emission. We simulate BBHs merging at redshifts of  $z = 10, 20, 30, 40,$  and  $50$ . The total masses in the source frame are  $M_{\text{tot}} = 5, 10, 20, 40, 80, 160,$  and  $250 M_{\odot}$ , with mass ratios  $q = 1, 2, 3, 4,$  and  $5$  (where  $q \equiv m_1/m_2$  for  $m_1 > m_2$ ) and orbital inclination angles  $\iota = 0$  (face on),  $\pi/6, \pi/3,$  and  $\pi/2$  (edge on). The simulated BBHs are nonspinning, as it is expected that PBHs are born with negligible spins (De Luca et al. 2019; Mirbabayi et al. 2020) and may be spun up by accreting materials later in their lives (Bianchi et al. 2018; De Luca et al. 2020a, 2020b, 2020c). However, we do not assume zero spins when estimating the source parameters and instead allow for generic spin precession. For each of these 700 sources, the sky location and polarization angles are chosen to maximize the source’s signal-to-noise ratio (S/N).

In order to measure a source’s distance (and hence redshift<sup>10</sup>), one needs to disentangle the two GW polarizations. Thus, we consider networks of noncollocated next-generation observatories as opposed to single-site detectors. We work with two detector networks: (i) a 40 km CE in the United States and an ET in Europe (CE–ET) and (ii) a CE–ET with an additional 20 km CE in Australia (CE–CES–ET). We only analyze sources whose network S/Ns are larger than 12. Generally speaking, BBHs with  $q \geq 5$  and  $M_{\text{tot}} \geq 160 M_{\odot}$  or  $M_{\text{tot}} \leq 5 M_{\odot}$  can only be detected up to  $z \sim 20$ . Because the sensitivity of ET (ET Design Team 2018) is better than that of CE (Evans et al. 2021c) below 10 Hz, the network S/N is dominated by ET instead of CE for  $M_{\text{tot}} \gtrsim 40 M_{\odot}$  (Evans et al. 2021b).

We obtain posterior probability densities with the nested sampling method developed and implemented by Skilling (2006) and Speagle (2020) using BILBY (Ashton et al. 2019). The inference is made with a zero-noise realization (Vallisneri 2008) because we are only interested in the uncertainty caused by the limited S/N and discard the offsets potentially caused by Gaussian fluctuations (Rodriguez et al. 2014). We employ the IMRPhenomXPHM waveform, which accounts for the effects of spin precession and higher-order modes (HoMs; Pratten et al. 2021), both to create the simulated waveforms and to calculate the likelihood. It is necessary to include HoMs in our analysis as they are important for systems with large detector-frame masses ( $\gtrsim 100 M_{\odot}$ ) and large mass ratios. In particular, their presence may help break the distance–inclination degeneracy characteristic of

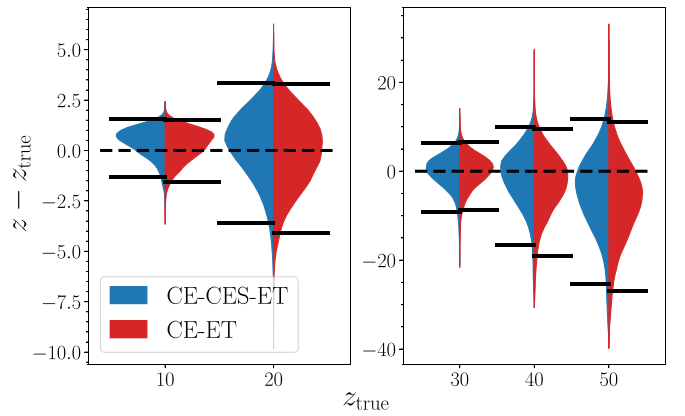


**Figure 1.** Redshift posteriors (offset by the true values) for sources with  $(M_{\text{tot}}, q, \iota) = (40M_{\odot}, 1, \pi/6)$  at five different redshifts observed by CE–ET (red) and CE–CES–ET (blue). The solid horizontal lines show the 95% credible intervals, whereas the dashed lines mark  $z_{\text{true}}$ .

the dominant (2, 2) harmonic mode (Chen et al. 2019; Usman et al. 2019). We find it more efficient to sample the parameter space with uniform priors in the detector-frame total mass,  $M_{\text{tot}}(1+z)$ , and  $q$ . The posteriors obtained this way are then reweighted into uniform priors in the source-frame primary mass,  $m_1$ , and the inverse mass ratio  $1/q$  (which is between 0 and 1). The default prior on redshift is constant in the comoving rate density,  $p_0(z) \propto \frac{dV_c}{dz} \frac{1}{1+z}$ , but we will explore other options below. We used isotropic priors for the sky position, the orbital and spin orientations. Uniform priors were used for the arrival time, phase of the signal at the time of arrival, and the spin magnitude. Unless otherwise specified, in what follows we quote uncertainties at 95% credible intervals.

## 3. Redshift Uncertainties

Figure 1 shows the redshift posteriors for a BBH system with  $(M_{\text{tot}}, q, \iota) = (40M_{\odot}, 1, \pi/6)$  located at different redshifts (given in the x-axis), as observed by CE–ET (red) and CE–CES–ET (blue). To increase the resolution along the y-axis, we have offset each posterior by the true redshift. The uncertainty increases with the true redshift, from  $\Delta z \sim 5$  at  $z_{\text{true}} = 10$  to  $\Delta z \sim 30$  at  $z_{\text{true}} = 50$ , for a CE–CES–ET network.

The roughly linear increase of the uncertainty with redshift is not just due to the reduction of the signal’s amplitude, as it happens for the sources discovered by advanced detectors. For any frequency in the inspiral phase of the waveform, the Fourier amplitude is proportional to  $[(1+z)\mathcal{M}_c]^{5/6} d_L^{-1}$ , where  $\mathcal{M}_c$  is the source-frame chirp mass and  $d_L$  is the luminosity distance. At large redshifts,  $d_L \propto (1+z)$ . Thus, for a given  $\mathcal{M}_c$ , the inspiral Fourier amplitude of sources at  $z \gg 1$  only falls off as  $(1+z)^{-1/6}$ . However, the loss in S/N at higher redshifts is greater because frequencies are redshifted by a factor of  $(1+z)$  where the detectors’ sensitivity might be poorer but also because signals have smaller bandwidth in the detectors’ sensitive range. These effects add up to yield the trend observed in Figure 1.

We also note that the network without CES yields uncertainties that are up to  $\sim 10\%$  larger than the three-detector network. This happens because an extra detector improves the resolution of the GW polarizations.

Next, we discuss how the redshift uncertainty depends on the total mass of the system. In Figure 2 we show the redshift posteriors of BBHs of increasing  $M_{\text{tot}}$ , with  $z_{\text{true}} = 40, q = 1,$

<sup>10</sup> Throughout this study, we use a  $\Lambda$ CDM cosmology based on the Planck 2018 results (Aghanim et al. 2020) to convert luminosity distance into redshift.

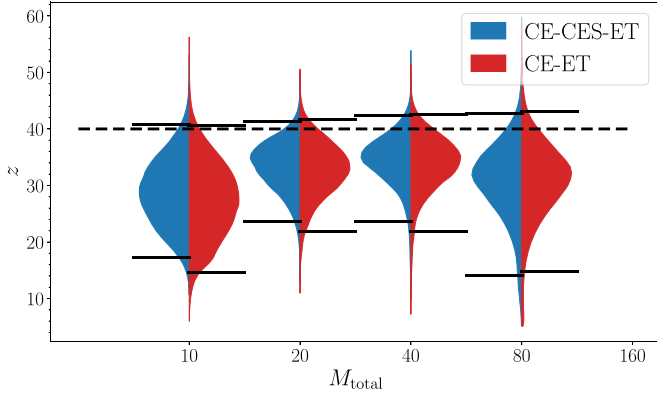


**Figure 2.** Redshift posteriors for sources with  $(q, l, z) = (1, 0, 40)$  at four different total masses observed by CE-ET (red) and CE-CES-ET (blue). The solid horizontal lines show the 95% credible intervals, whereas the dashed line marks  $z_{\text{true}}$ . Only sources with  $S/N \geq 12$  are included.

and  $l = 0$ . The uncertainty obtained by CE-CES-ET first decreases from  $\Delta z \sim 20$  for  $M_{\text{tot}} = 10M_{\odot}$  to  $\Delta z \sim 15$  for  $M_{\text{tot}} = 40M_{\odot}$ , then increases to  $\Delta z \sim 25$  for  $M_{\text{tot}} = 80M_{\odot}$  (this plot does not feature a system with  $M_{\text{tot}} = 5$  and  $160M_{\odot}$  as its  $S/N$  is below the threshold of 12). The nonlinear trend apparent in this plot is the result of two competing effects. At first, as  $M_{\text{tot}}$  increases, so do the signal amplitude and the  $S/N$ . In this regime, the uncertainty decreases with  $M_{\text{tot}}$ . However, when  $M_{\text{tot}}$  increases further, signals sweep less of the detectors’ sensitive bandwidth. In this regime, the uncertainties increase with  $M_{\text{tot}}$ .

We also notice an offset between the true redshift and the maximum a posteriori redshift of each source. There are two reasons for this offset. The default redshift prior goes as  $p_0(z) \sim (1+z)^{-5/2}$  in the matter-dominated regime,  $1 \lesssim z \lesssim 1000$ , hence favoring lower redshifts. Furthermore, the true inclination of these sources is 0, which implies that underestimating the redshift can be compensated for by measuring inclination angles closer to edge on. The opposite is impossible because the true inclination is at the edge of its physically allowed prior. This can be readily seen from the anticorrelation between distance and inclination for a nearly face-on system ( $l \ll 1$ ) whose GW amplitudes of both plus and cross-polarizations scale with  $\sim (1 - l^2/2)/d_L$  (Chen et al. 2019; Usman et al. 2019). This asymmetry makes it easier to underestimate the redshift but more difficult to overestimate it. This is why this systematic offset was not observed in Figure 1, where the true inclination was  $\pi/6$ .

#### 4. Ambiguity of a Single Event

With these results at hand, we now address the key question of this study: Can one pinpoint the redshift of merging BBHs to be above some threshold value? The answer clearly depends on which threshold is used. While the redshift at which the first stars were born is not precisely known, theoretical calculations and cosmological simulations suggest that the first stars might have been born at redshifts smaller than  $z \sim 40$  (Bromm 2006; de Souza et al. 2011; Koushiappas & Loeb 2017; Mocz et al. 2020).<sup>11</sup> Meanwhile, population synthesis models indicate that the characteristic time delay between formation and merger for Population III stars is  $\mathcal{O}(10)$  Myr (Kinugawa et al.

<sup>11</sup> Although we note that there are studies suggesting an earlier ( $z \gtrsim 50$ ; Trenti & Stiavelli 2009) or a later ( $z \lesssim 20$ ; Tornatore et al. 2007) formation of Population III stars.

**Table 1**  
Parameters of the Simulations that Result in a Probability of a Primordial Origin  $P_p \geq 0.9$ , Assuming the Default Prior  $p_0(z)$

$M_{\text{tot}}$	$q$	$l$	$z$	$\rho_{\text{CE}}$	$\rho_{\text{CES}}$	$\rho_{\text{ET}}$	$\rho_{\text{net}}$	$P_p$
20	1	0	50	16.6	7.2	5.9	19.1	0.93
20	1	$\pi/6$	50	14.0	6.3	5.2	16.2	0.94
20	2	0	50	13.6	5.8	5.2	15.7	0.95
20	2	$\pi/6$	50	11.6	5.1	4.5	13.5	0.91
20	3	0	40	13.0	5.7	4.5	14.9	0.92
40	1	$\pi/6$	40	7.4	6.9	16.8	19.6	0.91
40	1	$\pi/3$	40	6.0	4.6	9.5	12.1	0.97
40	1	0	50	3.0	4.2	17.8	18.5	0.94
40	1	$\pi/6$	50	2.6	3.5	15.1	15.7	0.96
40	2	0	40	5.6	6.0	17.2	19.0	0.92
40	2	0	50	2.1	3.0	14.5	15.0	0.93
40	3	0	40	3.2	4.0	13.7	14.7	0.91

**Note.** We also show the individual  $S/N$  in CE,  $\rho_{\text{CE}}$ ;  $S/N$  in CES,  $\rho_{\text{CES}}$ ;  $S/N$  in ET,  $\rho_{\text{ET}}$ ; as well as the network  $S/N$ ,  $\rho_{\text{net}}$ . The reason why the  $S/N$  in CES is sometimes larger than that in CE is discussed in Table 3 of the Appendix.

2014, 2016, 2020; Hartwig et al. 2016; Belczynski et al. 2017; Inayoshi et al. 2017; Liu & Bromm 2020a, 2020b; Tanikawa et al. 2021). This implies that the redshift at which Population III remnant BBHs merge is below  $z \sim 30$ . On the other hand, stellar-mass PBHs are expected to have formed at  $z \gg 1000$ , much earlier than the recombination epoch, and have been merging with one another since then (Raïdal et al. 2019). The PBH merger-rate density therefore increases monotonically with redshift (Raïdal et al. 2019), unlike that of ABHs.

Based on the above, we choose a critical redshift  $z_{\text{crit}} = 30$ , above which no astrophysical BBHs are expected to merge. We define the probability of primordial origin,  $P_p$ , as the fraction of the redshift posterior with  $z \geq z_{\text{crit}}$ . In the following, we only consider the measurements made by CE-CES-ET, which are always better than those made by CE-ET.

In Table 1, we list the BBH sources for which  $P_p \geq 0.9$ , and the corresponding values of  $P_p$  for  $z_{\text{crit}} = 30$  (see Table 3 in Appendix for  $z_{\text{crit}} = 20$ ). We find that only sources with  $z \geq 40$  and  $M_{\text{tot}} = 20M_{\odot}$  or  $40M_{\odot}$  achieve  $P_p \geq 0.9$ . We stress that the highest  $P_p$  are not reached by face-on sources, despite the fact that they have the largest  $S/N$ s. This is because the amplitude of HoMs is smallest for face-on sources, which will suffer the most from the distance–inclination degeneracy, and hence have larger uncertainties. We will explore this trade-off further in a forthcoming paper.

Next, we want to explore the dependence of these results on the redshift prior. The results presented thus far used our default redshift prior, the constant comoving rate density, given above. One could instead employ a prior informed by reasonable merger rates for ABHs and PBHs. In this case, the analysis of  $P_p$  answers the following question: Given some expected redshift distribution of the mergers of ABHs and PBHs, what is the probability that this system is primordial? To answer quantitatively, we adopt the merger-rate density for PBHs,  $\dot{n}_{\text{PBH}}(z) \propto \left(\frac{t(z)}{t(0)}\right)^{-34/37}$ , with  $t(z)$  the age of the universe at  $z$ , from Raïdal et al. (2017, 2019) and De Luca et al. (2020c), and that for the Population III BBH mergers,

$$\dot{n}_{\text{III}}(z) \propto \begin{cases} \frac{e^{a_{\text{III}}(z-z_{\text{III}})}}{b_{\text{III}} + a_{\text{III}}e^{(a_{\text{III}}+b_{\text{III}})(z-z_{\text{III}})}} & \text{if } z < z_{\text{crit}} \\ 0 & \text{otherwise,} \end{cases} \quad (1)$$

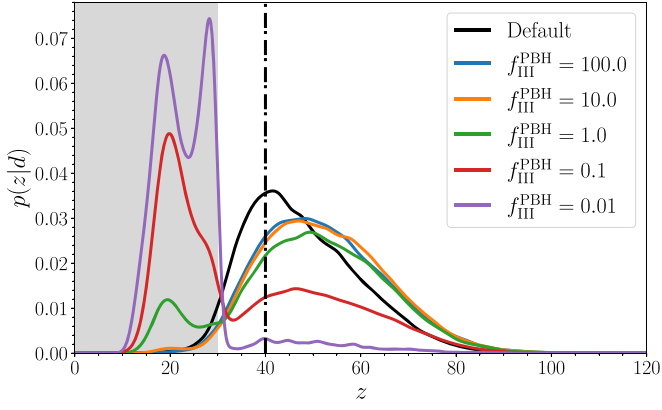


**Figure 3.** Posteriors of the system  $(M_{\text{tot}}, q, \iota, z) = (40M_{\odot}, 1, \pi/3, 40)$ , using  $p_{\text{tot}}(z)$  evaluated at  $f_{\text{III}}^{\text{PBH}} = 100$  (blue), 10 (orange), 1 (green), 0.1 (red), and 0.01 (purple). The black solid line shows the default posterior. The black dashed line indicates  $z_{\text{true}} = 40$ , and the gray area indicates the astrophysical region  $z < z_{\text{crit}}$ .

from Belczynski et al. (2017) and Ng et al. (2021), with  $(a_{\text{III}}, b_{\text{III}}, z_{\text{III}}) = (0.66, 0.3, 11.6)$  from Ng et al. (2021).

Then, we construct a mixture model for the merger-rate-based redshift prior,

$$p_{\text{tot}}(z|f_{\text{III}}^{\text{PBH}}) \propto \left[ f_{\text{III}}^{\text{PBH}} \frac{\dot{n}_{\text{PBH}}(z)}{\dot{n}_{\text{PBH}}(z_{\text{crit}})} + \frac{\dot{n}_{\text{III}}(z)}{\dot{n}_{\text{III}}(z_{\text{crit}})} \right] dV_c \frac{1}{dz} \frac{1}{1+z},$$

where  $f_{\text{III}}^{\text{PBH}}$  represents the ratio of the merger rate contributed by PBH mergers to that contributed by Population III BBH mergers at  $z_{\text{crit}}$ :  $f_{\text{III}}^{\text{PBH}} \equiv \dot{n}_{\text{PBH}}(z_{\text{crit}})/\dot{n}_{\text{III}}(z_{\text{crit}})$ . We plot  $p_{\text{tot}}(z|f_{\text{III}}^{\text{PBH}})$  for different values of  $f_{\text{III}}^{\text{PBH}}$  in the Appendix.

We then reanalyze the source with the largest  $P_p$  of Table 1, namely,  $(M_{\text{tot}}, q, \iota, z) = (40M_{\odot}, 1, \pi/3, 40)$ , by applying the rate-based redshift prior  $p_{\text{tot}}(z|f_{\text{III}}^{\text{PBH}})$  instead of the default prior  $p_0(z)$ . The redshift posteriors for different  $f_{\text{III}}^{\text{PBH}}$  are shown in Figure 3. When  $f_{\text{III}}^{\text{PBH}}$  decreases below 1, the posterior becomes bimodal with a low-redshift peak around  $z \approx 20$ , which becomes the dominating peak for  $f_{\text{III}}^{\text{PBH}} \lesssim 0.1$ . We tabulate the values of  $P_p$  for the same system, calculated with the different priors in Table 2. The value of  $P_p$  drops below 0.95 for  $f_{\text{III}}^{\text{PBH}} \leq 1$ . This seems to suggest that unless one believes a priori that the relative fraction between PBH mergers and Population III BBH mergers at  $z_{\text{crit}}$  is at least unity, the probability that a specific source is primordial can be made arbitrarily low.

However, not all priors need to yield comparable Bayesian evidences and one might use Bayesian evidences to identify strong priors that are disfavored by the data. Following Vitale et al. (2017), Zevin et al. (2020), and Bhagwat et al. (2021), one can thus calculate the Bayes factor  $\mathcal{B}_0^p = Z_p/Z_0$ , where  $Z_p$  and  $Z_0$  are the single-event evidences calculated with the rate-based prior and the default prior, respectively. Values of  $\mathcal{B}_0^p > 1$  imply that the default prior is disfavored. As shown in Table 2, the value of  $\mathcal{B}_0^p$  decreases from  $\sim 2$  to  $\sim 3 \times 10^{-3}$  with  $f_{\text{III}}^{\text{PBH}}$ , meaning that rate-based priors with a small PBH fraction  $f_{\text{III}}^{\text{PBH}} \lesssim 0.1$  are strongly disfavored when compared to the rate-based prior with  $f_{\text{III}}^{\text{PBH}} \gtrsim 1$ . Therefore, while an a priori belief

**Table 2**

Probabilities of a Primordial Origin  $P_p$  of the System  $(M_{\text{tot}}, q, \iota, z) = (40M_{\odot}, 1, \pi/3, 40)$  and the Bayes Factor  $\mathcal{B}_0^p$  against the Default Prior Calculated with the Rate-based Priors  $p_{\text{tot}}(z|f_{\text{III}}^{\text{PBH}})$  for Different PBH-to-Population III Merger-rate Ratios at  $z_{\text{crit}}, f_{\text{III}}^{\text{PBH}}$

$f_{\text{III}}^{\text{PBH}}$	$P_p$	$\mathcal{B}_0^p$
100	0.98	1.93
10	0.98	0.40
1	0.88	0.035
0.1	0.49	0.0030
0.01	0.11	0.0028
Default	0.97	1

**Note.** The value of  $P_p$  calculated with default prior  $p_0(z)$  is shown for comparison.

that the fraction of PBHs is low will move the redshift posterior to lower values, it will also yield a low Bayes factor that disfavors the model with a smaller  $f_{\text{III}}^{\text{PBH}}$ , if the likelihood distribution had significant support at redshift values that are suppressed by the prior. This should not be surprising, as it is exactly how the analysis can warn the analysts that their prior is in tension with the current set of data.

## 5. Discussion

In this Letter, we have simulated BBHs merging at  $z \geq 10$  and quantified the uncertainties in their redshifts as measured by networks of next-generation ground-based gravitational-wave detectors. We have used full Bayesian parameter estimation and a waveform model that accounts for both HoMs and spin precession. The relative redshift uncertainties are larger than  $\sim 10\%$  at  $z \geq 10$ , even for a three-detector network, CE–CES–ET. Assuming that no astrophysical BBHs can merge above  $z_{\text{crit}} = 30$  (see the Appendix for a lower threshold), we found that the typical redshift measurement is not precise enough to conclude with certainty that a single source is of primordial origin. Among the systems we simulated, the ones for which one can establish the primordial nature more strongly have  $M_{\text{tot}} = 20M_{\odot}$  or  $40M_{\odot}$  at  $z_{\text{true}} \geq 40$ . We find 12 out of 80 such systems for which  $90\% < p(z > z_{\text{crit}}) < 97\%$  assuming a constant comoving rate density and using a CE–CES–ET network. With a smaller CE–ET network, only 3 sources have  $90\% < p(z > z_{\text{crit}}) < 94\%$ . We have also verified that with a single ET observatory, one can reach  $p(z > z_{\text{crit}}) \sim 70\%$ . With a smaller set of targeted simulations, we have verified that with a single CE observatory one cannot set significant constraints. This is expected as the capabilities of a single L-shaped detector to measure distances outside of a network are limited.

Next, we have shown how the redshift measurement depends significantly on the redshift prior used for the analysis. In particular, we have considered a prior informed by population synthesis and theoretical models and introduced a mixture model that allows for both ABHs and PBHs. As one would expect, the posterior probability of a primordial origin for a specific event decreases if the assumed prior ratio of a PBH merger rate to a Population III BBH merger rate is small. However, the Bayes factor between the mixture model and the

**Table 3**  
Same as Table 1 but with  $z_{\text{crit}} = 20$

$M_{\text{tot}}$	$q$	$\iota$	$z$	$\rho_{\text{CE}}$	$\rho_{\text{CES}}$	$\rho_{\text{ET}}$	$\rho_{\text{net}}$	$P_p$
10	1	0	40	12.1	5.8	3.7	13.9	0.92
10	1	0	50	11.3	5.4	3.4	13.0	0.98
20	1	0	30	22.7	10.6	7.0	26.0	0.96
20	1	0	40	19.9	8.5	6.0	22.5	1.00
20	1	0	50	16.6	7.2	5.9	19.1	0.99
20	2	0	30	19.4	9.0	6.2	22.3	0.99
20	2	0	40	16.5	7.3	5.5	18.9	0.99
20	2	0	50	13.6	5.8	5.2	15.7	0.99
20	3	0	30	15.7	7.2	5.1	18.0	0.98
20	3	0	40	13.0	5.7	4.5	14.9	1.00
20	4	0	30	13.0	5.8	4.4	14.9	0.98
20	5	0	30	11.0	4.9	3.8	12.6	0.99
20	1	$\pi/6$	30	19.7	8.7	5.7	22.3	0.96
20	1	$\pi/6$	40	17.0	7.3	5.1	19.2	0.99
20	1	$\pi/6$	50	14.0	6.3	5.2	16.2	1.00
20	2	$\pi/6$	30	17.3	7.6	5.0	19.6	0.95
20	2	$\pi/6$	40	14.2	6.1	4.4	16.1	0.99
20	2	$\pi/6$	50	11.6	5.1	4.5	13.5	0.99
20	3	$\pi/6$	30	14.3	6.2	4.3	16.1	0.97
20	3	$\pi/6$	40	11.1	5.0	4.0	12.8	0.99
20	4	$\pi/6$	30	11.7	5.5	4.1	13.5	0.97
20	1	$\pi/3$	30	13.1	5.7	3.3	14.7	0.98
20	1	$\pi/3$	40	11.2	4.7	3.0	12.5	1.00
20	2	$\pi/3$	30	12.2	5.4	3.0	13.7	0.95
40	1	0	30	27.6	12.6	13.3	33.1	0.98
40	1	0	40	8.8	8.2	19.8	23.2	0.99
40	1	0	50	3.0	4.2	17.8	18.5	0.99
40	2	0	30	21.5	10.1	12.2	26.8	0.98
40	2	0	40	5.6	6.0	17.2	19.0	0.98
40	2	0	50	2.1	3.0	14.5	15.0	0.98
40	3	0	30	14.6	7.8	11.5	20.2	0.96
40	3	0	40	3.2	4.0	13.7	14.7	0.98
40	4	0	30	10.1	6.2	10.7	16.0	0.97
40	5	0	30	7.6	5.0	9.5	13.2	0.99
40	1	$\pi/6$	30	23.0	10.8	12.0	28.1	0.98
40	1	$\pi/6$	40	7.4	6.9	16.8	19.6	0.99
40	1	$\pi/6$	50	2.6	3.5	15.1	15.7	0.99
40	2	$\pi/6$	30	19.2	9.0	10.5	23.7	0.93
40	2	$\pi/6$	40	5.2	5.6	14.9	16.8	0.96
40	2	$\pi/6$	50	2.2	3.0	12.8	13.3	0.98
40	3	$\pi/6$	40	3.4	4.2	12.2	13.4	0.96
40	4	$\pi/6$	30	10.2	6.3	9.4	15.2	0.92
40	1	$\pi/3$	30	15.3	6.9	6.6	18.0	1.00
40	1	$\pi/3$	40	6.0	4.6	9.5	12.1	1.00
40	2	$\pi/3$	30	13.8	6.3	5.9	16.3	0.97
40	1	$\pi/2$	30	11.5	4.6	2.8	12.7	1.00
80	1	0	30	2.7	4.5	29.1	29.5	0.98
80	1	0	40	0.8	1.4	14.1	14.2	0.93
80	2	0	30	1.9	3.2	22.4	22.7	0.97
80	3	0	30	1.2	2.0	15.7	15.9	0.94
80	1	$\pi/6$	30	2.3	3.8	24.6	25.0	0.99
80	1	$\pi/3$	30	1.3	2.7	14.8	15.1	1.00
80	2	$\pi/3$	30	1.4	3.0	13.4	13.8	0.97

**Note.** The reason why the S/N in the smaller CES detector is sometimes larger than in CE is because the sky position and polarization of each source are chosen to maximize the network S/N. For sources whose network S/N is dominated by the ET detector, the resulting values of the extrinsic parameters might yield a smaller S/N in the CE detector than in CES.

constant comoving density model also decreases. Claims based on individual events would thus benefit from better knowledge of the properties of Population III stars and their remnants, notably the highest rate at which they merge. Forthcoming facilities such as the James Webb Space Telescope, the Roman space telescope, or Euclid are expected to probe the properties of Population III stars by accessing Population III galaxies in blind surveys (Vikaeus et al. 2022). More information will be yielded by instruments such as SPHEREx, by precisely measuring the near-infrared background (Sun et al. 2021), and mission concepts like THESEUS, by detecting the most distant long gamma-ray burst (Tanvir et al. 2021).

While an event-by-event basis identification of PBH binaries might be challenging, one can find evidence for PBHs in the whole data set. There are two possible methods for performing such an analysis. First, the subthreshold events from PBH mergers may contribute to a distinctive stochastic GW background, whose amplitude is directly related to the rate of PBH mergers (Mukherjee et al. 2022). Second, one can combine their redshift measurements of all resolvable sources at high redshifts through hierarchical Bayesian analysis. This also allows for detailed modeling of the features of each subpopulation (Farr et al. 2015; Mandel et al. 2019; Thrane & Talbot 2019; Wysocki et al. 2019; Vitale 2020). We will explore this avenue in a future paper. Posterior samples of the simulated BBHs can be found in [10.5281/zenodo.6471402](https://doi.org/10.5281/zenodo.6471402).

We would like to thank E. Berti, M. Evans, G. Franciolini, P. Pani, M. Punturo, and A. Riotto for suggestions and comments. K.K.Y.N. and S.V. are supported by the NSF through award PHY-1836814. S.C. is supported by the Undergraduate Research Opportunities Program of the Massachusetts Institute of Technology. The work of M.M. is supported by the Swiss National Science Foundation and by the SwissMap National Center for Competence in Research. M.B. acknowledges support from the European Union’s Horizon 2020 Programme under the AHEAD2020 project (grant agreement No. 871158). B.S.S. is supported in part by NSF grant Nos. PHY-1836779, AST-2006384, and PHY-2012083. S.B. is supported by NSF grant No. PHY-1836779. B.G. is supported by the Italian Ministry of Education, University and Research within the PRIN 2017 Research Program Framework, n. 2017SYRTCN.

## Appendix

In Figure 4, we show  $p_{\text{tot}}(z|f_{\text{III}}^{\text{PBH}})$  for five different values of  $f_{\text{III}}^{\text{PBH}}$ . The appearance of the discontinuity at  $z_{\text{crit}}$  is caused by the piecewise nature of the Population III BBH merger-rate density in Equation (1) of this Letter.

Given that the peak of the merger rate for BBHs from Population III stars is at  $z \sim 12$  (Figure 4), one might explore values of  $z_{\text{crit}}$  lower than what we used in the body of the Letter. Below, we report a version of Table 1 obtained with a less conservative  $z_{\text{crit}} = 20$ . This results in a larger number of sources that clear the  $P_p > 0.9$  criterion and even yields sources for which all of the posterior is above  $z_{\text{crit}}$ .

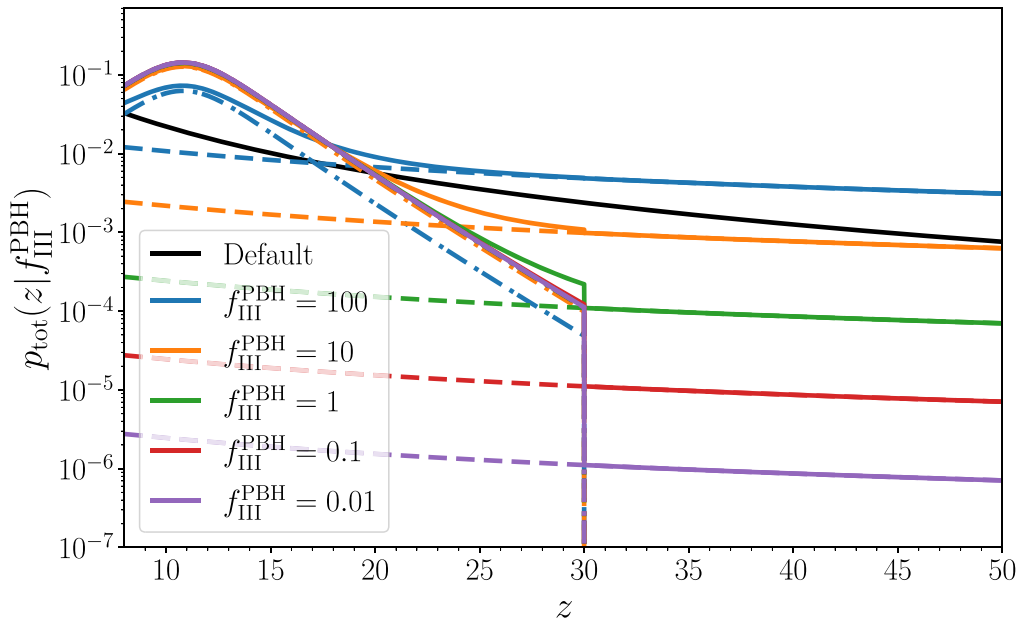


**Figure 4.** Prior based on the mixture model  $p_{\text{tot}}$  (solid lines), ranging from  $f_{\text{III}}^{\text{PBH}} = 100$  (blue), 10 (orange), 1 (green), 0.1 (red), and 0.01 (purple). The dashed lines and dashed-dotted lines represent the individual contribution from PBH mergers and Population III BBH mergers (which are truncated at  $z_{\text{crit}}$ ), respectively.

### ORCID iDs

Ken K. Y. Ng <https://orcid.org/0000-0003-3896-2259>  
 Boris Goncharov <https://orcid.org/0000-0003-3189-5807>  
 Ssohrab Borhanian <https://orcid.org/0000-0003-0161-6109>  
 Jan Harms <https://orcid.org/0000-0002-7332-9806>  
 Michele Maggiore <https://orcid.org/0000-0001-7348-047X>  
 B. S. Sathyaprakash <https://orcid.org/0000-0003-3845-7586>  
 Salvatore Vitale <https://orcid.org/0000-0003-2700-0767>

### References

- Aasi, J., Abbott, B. P., Abbott, R., et al. 2015, *CQGra*, **32**, 074001  
 Abbott, B. P., Abbott, R., Abbott, T. D., et al. 2017, *CQGra*, **34**, 044001  
 Abbott, R., Abbott, T. D., Abraham, S., et al. 2021, *PhRvX*, **11**, 021053  
 Acernese, F., Agathos, M., Agatsuma, K., et al. 2015, *CQGra*, **32**, 024001  
 Aghanim, N., Akrami, Y., Ashdown, M., et al. 2020, *A&A*, **641**, A6  
 Ali-Haïmoud, Y., Kovetz, E. D., & Kamionkowski, M. 2017, *PhRvD*, **96**, 123523  
 Antonini, F., & Giesles, M. 2020, *PhRvD*, **102**, 123016  
 Ashton, G., Hübner, M., Lasky, P. D., et al. 2019, *ApJS*, **241**, 27  
 Aso, Y., Michimura, Y., Somiya, K., et al. 2013, *PhRvD*, **88**, 043007  
 Bartos, I., Kocsis, B., Haiman, Z., & Márka, S. 2017, *ApJ*, **835**, 165  
 Bavera, S. S., Fragos, T., Qin, Y., et al. 2020, *A&A*, **635**, A97  
 Belczynski, K., Holz, D. E., Bulik, T., & O’Shaughnessy, R. 2016, *Natur*, **534**, 512  
 Belczynski, K., Ryu, T., Perna, R., et al. 2017, *MNRAS*, **471**, 4702  
 Belotsky, K. M., Dokuchaev, V. I., Eroshenko, Y. N., et al. 2019, *EPJC*, **79**, 246  
 Bhagwat, S., De Luca, V., Franciolini, G., Pani, P., & Riotto, A. 2021, *JCAP*, **01**, 037  
 Bianchi, E., Gupta, A., Haggard, H. M., & Sathyaprakash, B. S. 2018, arXiv:1812.05127  
 Breivik, K., Coughlin, S., Zevin, M., et al. 2020, *ApJ*, **898**, 71  
 Broekgaarden, F. S., Justham, S., de Mink, S. E., et al. 2019, *MNRAS*, **490**, 5228  
 Bromm, V. 2006, *ApJ*, **642**, 382  
 Carr, B., Raidal, M., Tenkanen, T., Vaskonen, V., & Veermäe, H. 2017, *PhRvD*, **96**, 023514  
 Carr, B. J., & Hawking, S. 1974, *MNRAS*, **168**, 399  
 Chen, H.-Y., Vitale, S., & Narayan, R. 2019, *PhRvX*, **9**, 031028  
 Chen, Z.-C., & Huang, Q.-G. 2018, *ApJ*, **864**, 61  
 Clesse, S., & García-Bellido, J. 2017, *PDU*, **15**, 142  
 De Luca, V., Desjacques, V., Franciolini, G., Malhotra, A., & Riotto, A. 2019, *JCAP*, **05**, 018  
 De Luca, V., Franciolini, G., Pani, P., & Riotto, A. 2020a, *PhRvD*, **102**, 043505  
 De Luca, V., Franciolini, G., Pani, P., & Riotto, A. 2020b, *JCAP*, **04**, 052  
 De Luca, V., Franciolini, G., Pani, P., & Riotto, A. 2020c, *JCAP*, **06**, 044  
 De Luca, V., Franciolini, G., Pani, P., & Riotto, A. 2021a, *JCAP*, **2021**, 039  
 De Luca, V., Franciolini, G., Pani, P., & Riotto, A. 2021b, *JCAP*, **05**, 003  
 de Mink, S., & Belczynski, K. 2015, *ApJ*, **814**, 58  
 de Souza, R. S., Yoshida, N., & Ioka, K. 2011, *A&A*, **533**, A32  
 Di Carlo, U. N., Giacobbo, N., Mapelli, M., et al. 2019, *MNRAS*, **487**, 2947  
 Dominik, M., Belczynski, K., Fryer, C., et al. 2012, *ApJ*, **759**, 52  
 Dominik, M., Belczynski, K., Fryer, C., et al. 2013, *ApJ*, **779**, 72  
 Dominik, M., Berti, E., O’Shaughnessy, R., et al. 2015, *ApJ*, **806**, 263  
 ET Design Team 2018, Power Spectral Density of Einstein Telescope, <https://tds.virgo-gw.eu/?content=3&r=14065>  
 Evans, M., Adhikari, R. X., Afle, C., et al. 2021a, A Horizon Study for Cosmic Explorer Science, Observatories, and Community, <http://dcc.cosmicexplorer.org/CE-P2100003/public>  
 Evans, M., Adhikari, R. X., Afle, C., et al. 2021b, arXiv:2109.09882  
 Evans, M., Adhikari, R. X., Afle, C., et al. 2021c, A Horizon Study for Cosmic500 Explorer Science, Observatories, and Community, [https://dcc.cosmicexplorer.org/public/0163/T2000017/004/ce\\_strain.txt](https://dcc.cosmicexplorer.org/public/0163/T2000017/004/ce_strain.txt)  
 Farr, W. M., Gair, J. R., Mandel, I., & Cutler, C. 2015, *PhRvD*, **91**, 023005  
 Franciolini, G., Baibhav, V., De Luca, V., et al. 2022, *PhRvD*, **105**, 083526  
 García-Bellido, J., Linde, A. D., & Wands, D. 1996, *PhRvD*, **54**, 6040  
 Green, A. M., & Kavanagh, B. J. 2021, *JPhG*, **48**, 043001  
 Gröbner, M., Ishibashi, W., Tiwari, S., Haney, M., & Jetzer, P. 2020, *A&A*, **638**, A119  
 Hall, E. D., & Evans, M. 2019, *CQGra*, **36**, 225002  
 Hartwig, T., Volonteri, M., Bromm, V., et al. 2016, *MNRAS*, **460**, L74  
 Hawking, S. 1971, *MNRAS*, **152**, 75  
 Hütsi, G., Raidal, M., Vaskonen, V., & Veermäe, H. 2021, *JCAP*, **03**, 068  
 Inayoshi, K., Hirai, R., Kinugawa, T., & Hotokezaka, K. 2017, *MNRAS*, **468**, 5020  
 Ioka, K., Chiba, T., Tanaka, T., & Nakamura, T. 1998, *PhRvD*, **58**, 063003  
 Ivanov, P. 1998, *PhRvD*, **57**, 7145  
 Ivanov, P., Naselsky, P., & Novikov, I. 1994, *PhRvD*, **50**, 7173  
 Khlopov, M. Y. 2010, *RAA*, **10**, 495  
 Kinugawa, T., Inayoshi, K., Hotokezaka, K., Nakauchi, D., & Nakamura, T. 2014, *MNRAS*, **442**, 2963  
 Kinugawa, T., Miyamoto, A., Kanda, N., & Nakamura, T. 2016, *MNRAS*, **456**, 1093  
 Kinugawa, T., Nakamura, T., & Nakano, H. 2020, *MNRAS*, **498**, 3946  
 Koushiappas, S. M., & Loeb, A. 2017, *PhRvL*, **119**, 221104  
 Kremer, K., Spera, M., Becker, D., et al. 2020, *ApJ*, **903**, 45

- Liu, B., & Bromm, V. 2020a, [ApJL](#), **903**, L40
- Liu, B., & Bromm, V. 2020b, [MNRAS](#), **495**, 2475
- Maggiore, M., Van Den Broeck, C., Bartolo, N., et al. 2020, [JCAP](#), **03**, 050
- Mandel, I., Farr, W. M., & Gair, J. R. 2019, [MNRAS](#), **486**, 1086
- Mapelli, M., Giacobbo, N., Santoliquido, F., & Artale, M. C. 2019, [MNRAS](#), **487**, 2
- Mirbabayi, M., Gruzinov, A., & Noreña, J. 2020, [JCAP](#), **03**, 017
- Mocz, P., Fialkov, A., Vogelsberger, M., et al. 2020, [MNRAS](#), **494**, 2027
- Mukherjee, S., Meinema, M. S. P., & Silk, J. 2022, [MNRAS](#), **510**, 6218
- Mukherjee, S., & Silk, J. 2021, [MNRAS](#), **506**, 3977
- Nakamura, T., Sasaki, M., Tanaka, T., & Thorne, K. S. 1997, [ApJL](#), **487**, L139
- Ng, K. K. Y., Vitale, S., Farr, W. M., & Rodriguez, C. L. 2021, [ApJL](#), **913**, L5
- O'Shaughnessy, R., Bellovary, J., Brooks, A., et al. 2017, [MNRAS](#), **464**, 2831
- Polnarev, A. G., & Khlopov, M. Y. 1985, [SvPhU](#), **28**, 213
- Portegies Zwart, S. F., & McMillan, S. L. W. 2000, [ApJL](#), **528**, L17
- Pratten, G., García-Quirós, C., Colleoni, M., et al. 2021, [PhRvD](#), **103**, 104056
- Punturo, M., Abernathy, M., Acernese, F., et al. 2010, [CQGra](#), **27**, 194002
- Raidal, M., Spethmann, C., Vaskonen, V., & Veermäe, H. 2019, [JCAP](#), **02**, 018
- Raidal, M., Vaskonen, V., & Veermäe, H. 2017, [JCAP](#), **09**, 037
- Reitze, D., Adhikari, R. X., Ballmer, S., et al. 2019, [BAAS](#), **51**, 35
- Rodriguez, C. L., Chatterjee, S., & Rasio, F. A. 2016, [PhRvD](#), **93**, 084029
- Rodriguez, C. L., Farr, B., Raymond, V., et al. 2014, [ApJ](#), **784**, 119
- Rodriguez, C. L., & Loeb, A. 2018, [ApJL](#), **866**, L5
- Rodriguez, C. L., Morscher, M., Pattabiraman, B., et al. 2015, [PhRvL](#), **115**, 051101
- Samsing, J., Bartos, I., D'Orazio, D., et al. 2020, [arXiv:2010.09765](#)
- Santoliquido, F., Mapelli, M., Giacobbo, N., Bouffanais, Y., & Artale, M. C. 2021, [MNRAS](#), **502**, 4877
- Sasaki, M., Suyama, T., Tanaka, T., & Yokoyama, S. 2016, [PhRvL](#), **117**, 061101
- Skilling, J. 2006, [BayAn](#), **1**, 833
- Speagle, J. S. 2020, [MNRAS](#), **493**, 3132
- Stevenson, S., Vigna-Gómez, A., Mandel, I., et al. 2017, [NatCo](#), **8**, 14906
- Sun, G., Mirocha, J., Mebane, R. H., & Furlanetto, S. R. 2021, [MNRAS](#), **508**, 1954
- Tagawa, H., Haiman, Z., Bartos, I., & Kocsis, B. 2020a, [ApJ](#), **899**, 26
- Tagawa, H., Haiman, Z., & Kocsis, B. 2020b, [ApJ](#), **898**, 25
- Tagawa, H., Kocsis, B., Haiman, Z., et al. 2021, [ApJ](#), **908**, 194
- Tanikawa, A., Susa, H., Yoshida, T., Trani, A. A., & Kinugawa, T. 2021, [ApJ](#), **910**, 30
- Tanvir, N. R., Le Floch, E., Christensen, L., et al. 2021, [ExA](#), **52**, 219
- Thrane, E., & Talbot, C. 2019, [PASA](#), **36**, e010
- Tornatore, L., Borgani, S., Dolag, K., & Matteucci, F. 2007, [MNRAS](#), **382**, 1050
- Trenti, M., & Stiavelli, M. 2009, [ApJ](#), **694**, 879
- Usman, S. A., Mills, J. C., & Fairhurst, S. 2019, [ApJ](#), **877**, 82
- Vallisneri, M. 2008, [PhRvD](#), **77**, 042001
- Vikaeus, A., Zackrisson, E., Schaerer, D., et al. 2022, [MNRAS](#), **512**, 3030
- Vitale, S. 2020, [arXiv:2007.05579](#)
- Vitale, S., Gerosa, D., Haster, C.-J., Chatziioannou, K., & Zimmerman, A. 2017, [PhRvL](#), **119**, 251103
- Wong, K. W. K., Franciolini, G., De Luca, V., et al. 2021, [PhRvD](#), **103**, 023026
- Wysocki, D., Lange, J., & O'Shaughnessy, R. 2019, [PhRvD](#), **100**, 043012
- Yang, Y., Bartos, I., Haiman, Z., et al. 2020, [ApJ](#), **896**, 138
- Yang, Y., Bartos, I., Gayathri, V., et al. 2019, [PhRvL](#), **123**, 181101
- Yi, S.-X., & Cheng, K. 2019, [ApJL](#), **884**, L12
- Zel'dovich, Y. B., & Novikov, I. D. 1966, [AZh](#), **43**, 758
- Zevin, M., Berry, C. P. L., Coughlin, S., Chatziioannou, K., & Vitale, S. 2020, [ApJL](#), **899**, L17